Ultrasonic analogue of surface plasmon polariton (SPP) electromagnetic waves in metamaterial waveguides

Piotr Kiełczyński

Institute of Fundamental Technological Research,
Polish Academy of Sciences,
ul. Pawińskiego 5B, 02-106 Warsaw, Poland.

e-mail: pkielczy@ippt.gov.pl

Abstract

The advent of elastic metamaterials at the beginning of the 21st century opened new venues and possibilities of existence for new types of acoustic (ultrasonic) waves, which were deemed previously impossible. In fact, it was commonly agreed that shear horizontal (SH) surface acoustic waves cannot exist on an elastic half-space or at the interface between two different elastic half-spaces. However, in this paper (inspired by the newly developed elastic metamaterials) we will show that SH surface elastic waves can propagate at the interface between two elastic half-spaces, provided that one of them is a metamaterial with a negative elastic compliance $s_{44}(\omega)$. In addition, if $s_{44}(\omega)$ changes with frequency ω as the dielectric function $\varepsilon(\omega)$ in Drude's model of metals, then the proposed SH ultrasonic waves can be considered as acoustic analogues of Surface Plasmon Polariton (SPP) electromagnetic waves propagating at the metal-dielectric interface. Due to inherent similarities between the proposed SH acoustic waves and SPP electromagnetic waves the new results developed in this paper can be readily transferred into the SPP domain and vice-versa. The proposed new SH ultrasonic surface waves are characterized by a strong subwavelength confinement of energy in the vicinity of the guiding interface, thus they can potentially be used in subwavelength acoustic imaging, superlensing and/or acoustic sensors with extremely large mass sensitivity.

Keywords: Metamaterial Elastic Waveguides, Negative Elastic Compliance, Shear Hotizontal (SH) Elastic Surface Waves, SPP Electromagnetic Waves, Phase and Group Velocity, Penetration Depth, Complex Power Flow

1. Introduction

Acoustic surface waves that exist in solid waveguides have seemingly very little in common with Surface Plasmon Polariton (SPP) electromagnetic waves propagating in metal-dielectric waveguides. However, with the advent of elastic metamaterials this assertion has to be revisited.

Indeed, one can argue that the invention of metamaterials was one of the most significant events in physics at the turn of the XX and XXI Century [1-2]. In fact, metamaterials challenged many tacit assumptions and believes accumulated in decades about properties of matter and wave motion herein. Combining basic research with a judicious engineering design, researchers devised a large number of new materials with unprecedented properties. In the domain of elastic media we observed emergence of elastic metamaterials with a negative mass density [3-5], anisotropic mass density [6], negative elastic constants [7-8], etc. Not surprisingly, these new properties opened possibilities for existence of new types of acoustic waves, which were previously considered as impossible.

Up to date it was commonly agreed that shear horizontal (SH) acoustic surface waves cannot exist at the interface between two elastic half-spaces [9]. In the submitted manuscript we challenge the above assertion, showing that SH acoustic (ultrasonic) surface waves can exist at the interface between two elastic-half-spaces, provided that one of them is elastic metamaterial with special properties, i.e., with a negative shear elastic compliance.

Consequently, in this paper we propose (inspired by the newly developed elastic metamaterials) a new type of shear horizontal (SH) acoustic surface waves that were previously deemed impossible [9], i.e., the waves that can propagate at the interface between two elastic half-spaces one of which is a metamaterial with a negative elastic compliance $s_{44}(\omega) < 0$. If, in addition, the compliance $s_{44}(\omega)$ changes with angular frequency ω as the dielectric function $\varepsilon(\omega)$ in Drude's model of metals, the proposed SH acoustic waves can be considered as ultrasonic analogues of Surface Plasmon Polariton (SPP) electromagnetic waves propagating at the metal-dielectric interface.

As a result, special attention was paid in this paper to similarities between the new proposed SH elastic surface waves and the electromagnetic surface waves of the surface plasmon polariton (SPP) type, propagating at a dielectric-metal interface [10-12]. In fact, SPP surface waves are transverse magnetic (TM) electromagnetic modes with only one transverse component, namely the magnetic field H_3 that is analogue of the SH mechanical displacement u_3 of the new proposed SH acoustic surface wave. It is noteworthy that both types of waves share one crucial property, i.e., very strong subwavelength decay in the transverse direction away from the guiding interface $x_2 = 0$ (see Fig.1).

Due to strong formal similarities between SPP electromagnetic surface waves and the new proposed SH elastic surface waves, most of the results obtained in this paper can be transferred directly into the SPP domain (see Table 1 in Section 4) and vice-versa. Many new interesting phenomena observed in the SPP domain, such as trapping of light (zero group velocity) [13], transformational optics systems [14] or nonreciprocal and topological waveguides [15] may be transferred into the domain of elastic metamaterial waveguides, using to this end the new SH acoustic surface waves proposed in this paper. Therefore, the proposed new SH acoustic surface waves open new possibilities to control wave phenomena in elastic solids.

The new ultrasonic wave has the character of a surface wave because it is an evanescent wave, (i.e. it decays exponentially) in the direction of the x_2 axis, perpendicular to the interface ($x_2 = 0$) and perpendicular to the direction of propagation x_1.

The proposed new SH acoustic surface waves can have deeply subwavelength penetration depth, in both half-spaces of the waveguide, therefore they offer a potential for applications in subwavelength acoustic imaging, superlensing and/or acoustic sensors with extremely large sensitivity, analogously to their SPP counterparts in electromagnetism. These are very attractive properties of the newly discovered ultrasonic waves.

The frequency range, in which the new SH acoustic surface wave can propagate covers practically the range from several kHz to several MHz. The maximum wave frequency $\omega_{sp}/2\pi$ depends on the resonant frequency of local resonators ω_p and is given by the formula 24. For example, when an exemplary waveguide structure from Fig.1 consists of 1) the metamaterial upper half-space ($x_2 \leq 0$) based on ST-Quartz with embedded local resonators with a selected resonant frequency $\omega_p/2\pi = 1\ MHz$, and 2) conventional PMMA elastic lower half space ($x_2 \geq 0$), the maximum wave frequency equals approximately to $\omega_{sp}/2\pi = 143\ kHz$ (according to the formula 24).

The application of the proposed new ultrasonic wave allows to achieve very high resolution (of the order of micrometers) using relatively low frequencies (of the order of a few MHz). So far, using conventional ultrasonic waves and imaging systems a similar resolution could be achieved using frequencies of the order of 1 GHz, what is very difficult.

The exciting properties of newly discovered ultrasonic waves are that they can slow down to zero (ω_{sp} and $\omega_{sp} \to 0$), when the wave frequency tends to the frequency ω_{sp}. This phenomenon generates concentration of energy near the interface what can be of crucial importance in subwavelength acoustic imaging,

acoustic energy harvesting as well as in miniaturized modern acoustic devices at the micro and nano-scale.

A number of analytical equations developed in this paper are new and original. As a result, they can provide fresh physical insight into the wave phenomena occurring in both domains, namely SPP electromagnetic waves and SH elastic surface waves. For example, Eqs. 30, 33, 36 and 37 that relate complex power flow with penetration depths in both half-spaces of the waveguide, were to the best of our knowledge not yet published in the literature. Table 1 in Section 4 provides corresponding field quantities in both analyzed domains.

The layout of this paper is as follows. Section 2.1 introduces the geometry and material parameters of two half-spaces forming the metamaterial waveguide. Section 2.2 describes properties of the metamaterial half-space with a negative elastic compliance $s_{44}^{(1)}(\omega) < 0$. Section 2.3 contains an acoustic model of a metamaterial, whose elastic compliance $s_{44}(\omega)$ obeys the Drude relation. Mechanical displacement u_3 and shear stresses τ_{13}, τ_{23} are subject of Section 3.1. Boundary conditions and the dispersion equation of the new SH waves is presented in Section 3.2. The formula for the wavenumber $k(\omega)$ was derived in Section 3.3. The formulas for the phase $v_p(\omega)$ and group $v_g(\omega)$ velocities were developed, in Sections 3.4 and 3.5, respectively. The equations for the penetration depth in both half-spaces are given in Section 3.6. The active power P_1 flow of, in the direction of propagation x_1, was determined in Section 3.7. The reactive power P_2 flow, in the transverse direction x_2 was analyzed in Section 3.8. The correspondence between SPP electromagnetic surface waves and the proposed new SH acoustic surface waves is outlined in Section 4. The results of numerical calculations and the corresponding figures are presented in Section 5. The discussion and conclusions are the subject of Sections 6 and 7, respectively.

2. Physical model

2.1 Geometry and material parameters of the waveguide

The geometry of the waveguide supporting new SH elastic surface waves is sketched in Fig.1. The waveguide consists of two semi-infinite elastic half-spaces, one of which is a conventional elastic material $(x_2 \geq 0)$ and the second an elastic metamaterial $(x_2 < 0)$ with a negative elastic compliance $s_{44}^{(1)}(\omega) < 0$, which is a function of angular frequency ω. By contrast, the densities $(\rho_1, \rho_2) > 0$ in both half-spaces as well as the elastic compliance $s_{44}^{(2)} > 0$ in the conventional elastic material are positive and frequency independent (see Fig.1).

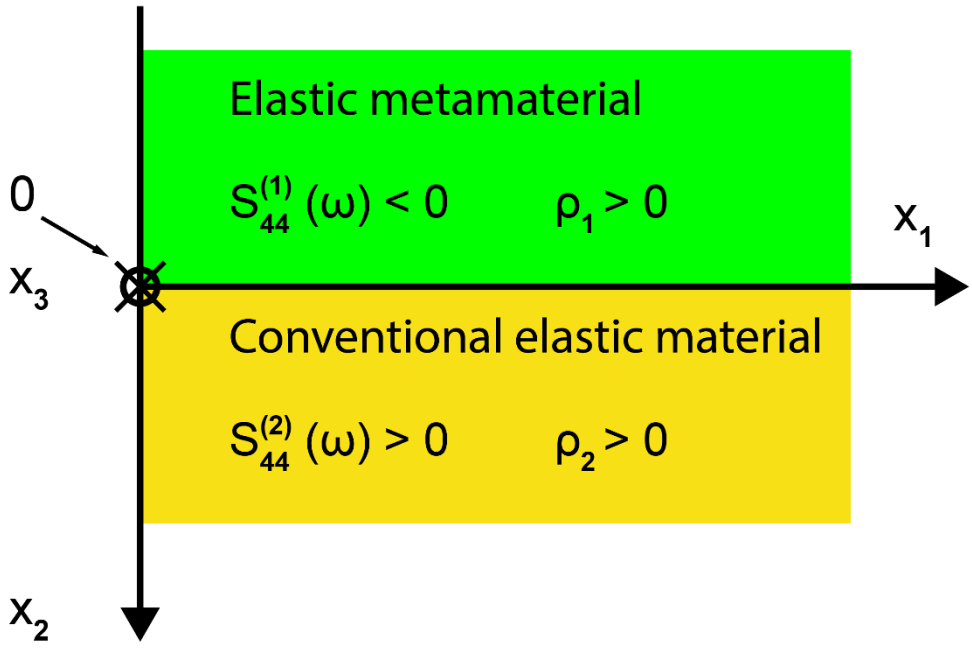

Fig.1 Cross-section of the waveguide supporting the newly proposed SH elastic surface waves, propagating in the direction x_1, with exponentially decaying fields in the transverse direction x_2. The conventional elastic half-space $(x_2 \geq 0)$ is rigidly bonded to the metamaterial elastic half-space $(x_2 < 0)$ at the interface $x_2 = 0$. Mechanical displacement u_3 of the new SH elastic surface waves is polarized along x_3

Two elastic half-spaces, rigidly bonded at the interface $x_2 = 0$, are uniform in the direction x_3, therefore all field quantities of the new SH elastic surface wave will vary only along the transverse direction x_2, i.e., as a function of distance from the guiding interface $x_2 = 0$. It is assumed that both half-spaces of the waveguide are linear and lossless.

2.2 Elastic compliance $s_{44}^{(1)}(\omega)$ in the metamaterial half-space ($x_2 < 0$)

The important assumption made throughout this paper is about the elastic compliance $s_{44}^{(1)}(\omega)$ in the metamaterial half-space ($x_2 < 0$). Namely, it is assumed that $s_{44}^{(1)}(\omega)$, as a function of angular frequency ω, is given explicitly by the following formula:

$$s_{44}^{(1)}(\omega) = s_0 \cdot \left(1 - \frac{\omega_p^2}{\omega^2}\right) \tag{1}$$

where: ω_p is the angular frequency of the local mechanical resonances of the metamaterial and s_0 is its reference elastic compliance for $\omega \to \infty$.

It is not difficult to notice that the elastic compliance $s_{44}^{(1)}(\omega)$ given by Eq.1, is formally identical to the dielectric function $\varepsilon(\omega)$ in Drude's model of metals [16], in which the angular frequency ω_p is named the angular frequency of bulk plasmon resonance [17].

Similarly, the density ρ_1 of the metamaterial half-space ($x_2 < 0$) corresponds to the magnetic permeability μ in Drude's model of metals.

The second elastic half-space ($x_2 < 0$) is a conventional elastic material with a positive compliance $s_{44}^{(2)} > 0$ and density $\rho_2 > 0$ that are both frequency independent.

2.3 The Drude–like behavior of mechanical systems

In order to justify the existence of elastic bodies whose elastic properties show the Drude type dependence on the angular frequency ω, we will use 1) a set of electromechanical analogies and 2) the similarity of the new ultrasonic waves of the SH type to electromagnetic waves of the Surface Plasmon Polariton (SPP) type, which propagate at the metal - dielectric interface.

The correspondence of the new SH ultrasonic waves to electromagnetic waves of the (SPP) type is due to the fact that they share the common mathematical model. Namely, the equations of motion (second Newton's law) describing the behavior of an elastic continuum (with parameters s_{44} and ρ) are analogous to Maxwell's equations describing the behavior of a continuous medium with parameters ε and μ.

This is the origin of the analogy between dielectric permeability and magnetic permeability and shear modulus and density: $\varepsilon \Leftrightarrow s_{44}$ and $\mu \Leftrightarrow \rho$, see Table 1 on page 21, which we can observe by analyzing the properties of mechanical surface SH waves and electromagnetic surface waves of the SPP type.

Therefore, the relationships that we prove in the electromagnetic domain for ε and μ can be transferred to the relationships that are valid for s_{44} and ρ in the mechanical domain.

A one-dimensional mechanical model, whose elastic properties can be described by Drude's dependence on angular frequency ω, can be shown in Fig.2.

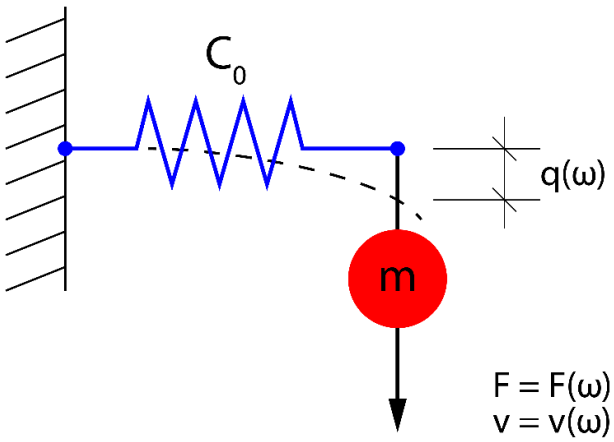

Fig.2. The spring-mass model of a mechanical resonator whose effective shear elastic constant $C_{eff}(\omega)$ varies on the angular frequency ω according to Drude's relation. $F(\omega)$ is the mechanical force, $q(\omega)$ is the mechanical displacement and $v(\omega) = j\omega q(\omega)$ is the acoustic velocity.

Figure 2. shows a one-dimensional mechanical resonator performing shear vibrations. The elementary resonator in Fig. 2 consists of an elastic spring with a compliance C_0 connected in series with mass m. The mechanical equivalent diagram and the electrical equivalent diagram of the system in Fig. 2 can be presented as follows, see Fig. 3a,b:

a) b)

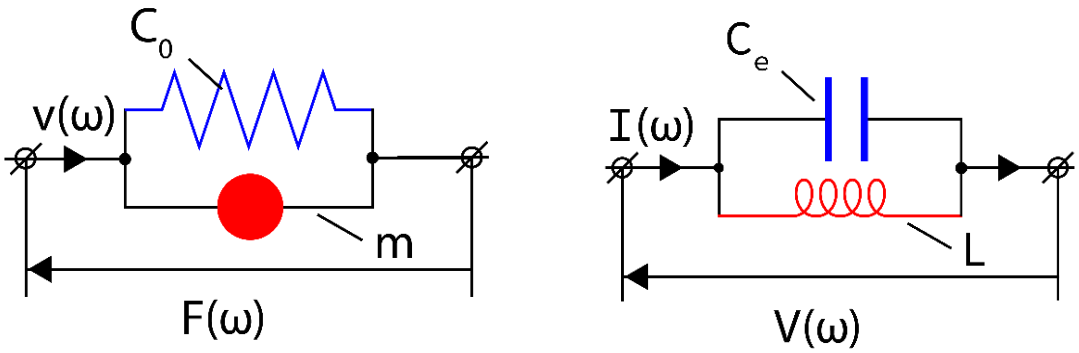

Fig.3 a) Mechanical equivalent circuit of the system from Fig. 2 and b) electrical equivalent circuit of the mechanical system from Fig.2. Here, $v(\omega)$ the acoustic velocity, $F(\omega)$ is the mechanical force, and C_0 is the elastic compliance of the spring.

The mechanical equivalent circuit in Fig. 3a can be analyzed in a similar way as the electrical equivalent circuit in Fig. 3b. The properties of the equivalent mechanical system from Fig. 3a will be investigated in the frequency ω domain.

Fig. 3a shows that the mechanical system in Fig. 2 is characterized by the following mechanical admittance $Y(\omega)$:

$$Y(\omega) = \frac{v(\omega)}{F(\omega)} = j\omega C_0 + \frac{1}{j\omega m} = j\omega C_0 \left(1 - \frac{\omega_0^2}{\omega^2}\right) \quad (2)$$

where: $\omega_0 = 1/\sqrt{mC_0}$ is the resonant frequency of the mechanical resonator.

As can be seen from Eq.2, the mechanical resonator shown in Fig.2 can be replaced by the resultant shear compliance $C_{eff}(\omega)$ represented by the spring, see Fig.4.

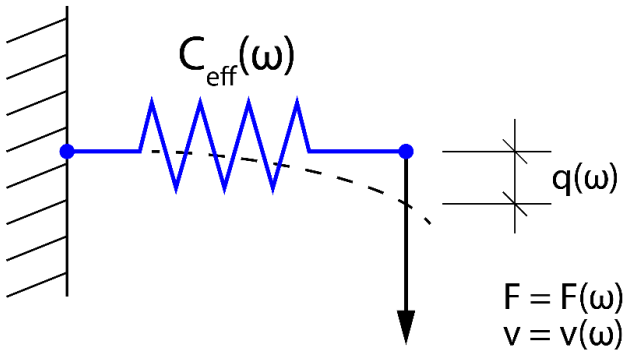

Fig.4. The equivalent elastic shear spring compliance $C_{eff}(\omega)$ that represents the overall mechanical behavior of the mechanical resonator from Fig.2.

The equivalent elastic shear spring compliance $C_{eff}(\omega)$ from Fig.4 is given by the following analytical formula:

$$C_{eff}(\omega) = C_0 \left(1 - \frac{\omega_0^2}{\omega^2}\right) \quad (3)$$

As can be seen from Eq.3, the frequency characteristic of the equivalent compliance $C_{eff}(\omega)$ is similar to the frequency dependence of the shear elastic compliance $s_{44}(\omega)$ described by Eq.1 on page 7, as well as to the dielectric constant $\varepsilon(\omega)$ described by the Drude formula in electromagnetism (optics).

The effective shear compliance $C_{eff}(\omega)$ is negative over a wide frequency range $(0 < \omega < \omega_0)$ below the resonant frequency $\omega_0 = 1/\sqrt{mC_0}$.

The frequency ω_0 corresponds to the plasma frequency of electrons in metals that are used in dielectric-metal layered waveguides in which Surface Plasmon Polariton (SPP) waves propagate (in the case of electromagnetism and optics).

This Drude-like behavior of the mechanical system from Fig.2 was the motivation to search for new ultrasonic surface SH waves, analogous to Surface Plasmon Polariton (SPP) electromagnetic waves, that propagate in elastic layered metamaterial waveguides, where the elastic shear compliance can exhibit a Drude-like dependence on angular frequency ω. This elementary cell (local oscillator) from Fig.2 can constitute the basis (microstructure) for the design and construction of metamaterials with the desired elastic properties.

As a unit cell that can be used as a local resonator, we choose the following structure, see Fig.5:

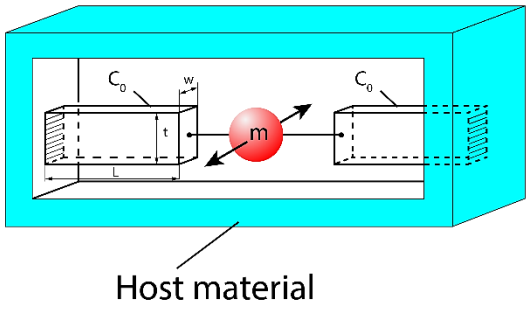

Fig.5. Practical realization of a local resonator performing shear vibrations.

The local resonator consists of a sphere of mass m mounted on 2 microcantilevers, which act as a spring with an effective compliance $C_0/2$. Microcatilevers are bonded to the host material. Elastic compliance of the microcantilever treated as a spring can be expressed as: $C_0 = 4L^3/Ewt^3$; where: L = length, w = width, t = height and Y = Young's modulus. The resonator performs shear oscillations in the direction perpendicular to Fig. 5 with the frequency $\omega_0 = \sqrt{2/mC_0}$.

The vibrational properties of local resonators of this type are revealed in the SH-type transverse shear wave field propagating in the bulk medium in which the set of these elementary oscillators, which perform shear vibrations, has been embedded.

The mean mechanical energy stored in the mechanical system represented by the mechanical equivalent diagram (mechanical two-port) in Fig. 3a equals:

$$W_M(\omega) = \frac{1}{4}\left(1 + \frac{\omega_0^2}{\omega^2}\right) \cdot C_0 \cdot |F|^2 \qquad (4)$$

Thus, from Equation 4, we can conclude that the mean mechanical energy density in a corresponding continuous elastic medium is equal to:

$$w_M(\omega) = \frac{1}{4}\left(1 + \frac{\omega_0^2}{\omega^2}\right) s_0 \cdot |\tau_{23}|^2 \qquad (5)$$

where: s_0 is the elastic compliance of the corresponding continuous elastic material, τ_{23} is the shear stress equal to: $\tau_{23} = F/A$, F is the shear force acting on the appropriate surface A of the local oscillator, see Fig. 6:

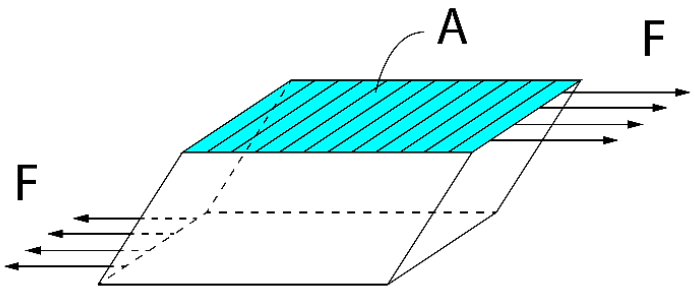

Fig.6. An elementary resonator performing shear vibrations. The shear force F is acting on the surface A of the resonator.

Therefore, the mechanical energy stored in the reference volume V in the elastic metamaterial is:

$$\frac{1}{4}\left(1+\frac{\omega_0^2}{\omega^2}\right)(s_0)^{eff}|\tau_{23}|^2\cdot V=\frac{1}{4}\left(1+\frac{\omega_0^2}{\omega^2}\right)\cdot n\cdot C_0\cdot|F|^2 \quad (6)$$

where: n is the number of local resonators contained in the reference volume V. The coefficient $(s_0)^{eff}$ in Eq.6 represents the averaged value of the elastic compliance of the resultant elastic metamaterial.

The relation for energy density in electromagnetic continuous media, whose material parameters exhibit a dependence on angular frequency ω, was developed by Ginzburg in [18]. From the analogy between mechanical and electromagnetic waves (see Table 1, lines No 4 and 5, i.e., the correspondence between $\varepsilon(\omega)$ and $s_{44}(\omega)$), we can write [18]:

$$\frac{d}{d\omega}\left(\omega\frac{s_{44}(\omega)}{(s_0)^{eff}}\right)=\left(1+\frac{\omega_0^2}{\omega^2}\right) \quad (7)$$

Performing integration on ω of both sides of Eq.7, we arrive at the following formula:

$$\frac{s_{44}(\omega)}{(s_0)^{eff}}=\left(1-\frac{\omega_0^2}{\omega^2}\right) \quad (8)$$

Equation 8 is the Drude's relation describing the elastic compliance $s_{44}(\omega)$ of the resulting elastic metamaterial as a function of angular frequency ω.

Knowing that: $|\tau_{23}|=|F|/A$, where A is the surface of the elementary resonator upon which the force F is acting and comparing left and right sides of Eq. 6, we can write:

$$(s_0)^{eff}=\frac{n\cdot C_0|F|^2}{|\tau_{23}|^2\cdot V}=\frac{n\cdot C_0\cdot A^2}{V} \quad (9)$$

Based on the performed analysis, an examplary model of an elastic metamaterial whose shear elastic compliance $s_{44}(\omega)$, as a function of angular frequency ω, varies according to the Drude relation can be presented as follows, see Fig. 7.

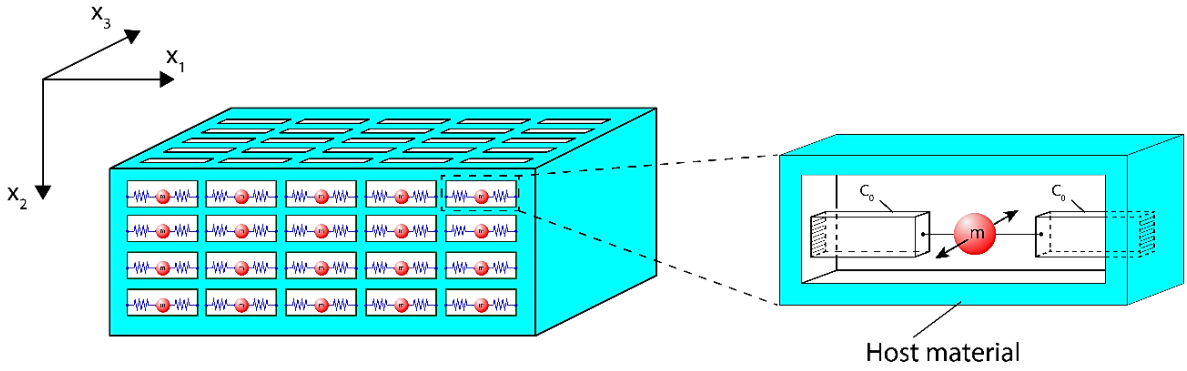

Fig. 7. A model of an elastic metamaterial with Drude-like dependence of elastic compliance $s_{44}(\omega)$ on angular frequency ω. A set of n local mechanical oscillators is embedded into the host material in the reference volume V. The inset shows details of an elementary (local) resonator.

3. Mathematical model

3.1 Mechanical displacement $u_3^{(i)}(x_2)$ and stresses $\tau_{23}^{(i)}(x_2)$, $\tau_{13}^{(i)}(x_2)$

Since new SH elastic surface waves are time-harmonic, propagate in the direction x_1 and are uniform along the transverse direction x_3, their mechanical displacement $u_3^{(i)}$, in both half-spaces ($i = 1,2$) shown in Fig.1, will be sought in the following generic form

$$u_3^{(i)} = u_3^{(i)}(x_2) exp[j(k \cdot x_1 - \omega t)] \tag{10}$$

where $u_3^{(i)}(x_2)$ expresses variations of the mechanical displacement in the transverse direction x_2, k is the wavenumber of the new SH elastic surface wave and ω its angular frequency.

The mechanical displacement $u_3^{(i)}$ in both half-spaces of the waveguide is governed by the wave equation, resulting from the second Newton's law, which with the help of Eq.10 reduces to the second order ordinary differential equation of the Helmholtz type [19]

$$\left[\frac{d^2}{dx_2} + k_i^2\right] \cdot u_3^{(i)}(x_2) = k^2 \cdot u_3^{(i)}(x_2) \tag{11}$$

where $k_i = \omega / v_i$ is the wavenumber of SH bulk waves in both elastic half-spaces number $i = 1, 2$. In the conventional elastic half-space ($i = 2$) the wavenumber $k_2^2 = \omega^2 s_{44}^{(2)} \rho_2$ is positive and in the metamaterial half-space ($i = 1$) the wavenumber $k_1^2 = -\omega^2 \left| s_{44}^{(1)} \right| \rho_1$ is always negative in the angular frequency range $0 < \omega \leq \omega_p$.

Since the mechanical displacement $u_3^{(i)}(x_2)$ of the new SH elastic surface wave must vanish at large distances from the guiding interface $x_2 = 0$, namely for $x_2 \to \pm\infty$, the solution of the Helmholtz Eq.11 will be sought in the following form

$$u_3^{(i)}(x_2) = C_i e^{\pm q_i x_2} \tag{12}$$

where C_i ($i = 1,2$) are arbitrary amplitude coefficients and the transverse wave numbers q_i are real (waveguide is lossless) and according to the Helmoltz Eq.11 are given by $q_i = \sqrt{(k^2 - k_i^2)}$, where $k_i = 1/\sqrt{s_{44}^{(i)} \rho_i}$ are wavenumbers of bulk SH waves in the metamaterial half-space $x_2 < 0$ ($i = 1$) and conventional elastic half-space $x_2 \geq 0$ ($i = 2$).

In the following of this paper we will use two shear stresses of the new SH elastic surface wave, namely $\tau_{23}^{(i)}$ and $\tau_{13}^{(i)}$ that are defined, respectively, as: $\tau_{23}^{(i)} = \left(1/s_{44}^{(i)}\right) \partial u_3^{(i)}/\partial x_2$ and $\tau_{13}^{(i)} = \left(1/s_{44}^{(i)}\right) \partial u_3^{(i)}/\partial x_1$.

Consequently, we can write the following formulas:

$$u_3^{(i)}(x_2) = C_i \cdot exp(\pm q_i x_2) \tag{13}$$

$$\tau_{23}^{(i)}(x_2) = \frac{1}{s_{44}^{(i)}} C_i \cdot q_i \cdot exp(\pm q_i x_2) \tag{14}$$

$$\tau_{13}^{(i)}(x_2) = \frac{1}{s_{44}^{(i)}} C_i \cdot jk \cdot exp(\pm q_i x_2) \tag{15}$$

$$q_i = \sqrt{(k^2 - k_i^2)} \tag{16}$$

where the index $i = 1,2$.

In order to provide an exponential decay of $u_3^{(i)}(x_2), \tau_{23}^{(i)}(x_2)$ and $\tau_{13}^{(i)}(x_2)$ the transverse wavenumber q_i in Eqs 13-16 have to be preceded by sign $-$ in the convention elastic half-space ($x_2 \geq 0$) and by sign $+$ in the metamaterial half-space ($x_2 < 0$), since q_i ($i = 1,2$) in Eqs. 13-16 are real and positive.

3.2 Boundary conditions and dispersion equation

From physical considerations it is obvious that the mechanical displacement $u_3^{(i)}(x_2)$ and the shear stress $\tau_{23}^{(i)}(x_2)$ have to be continuous at the interface $x_2 = 0$, namely:

$$u_3^{(1)}(x_2 = 0) = u_3^{(2)}(x_2 = 0) \tag{17}$$

$$\tau_{23}^{(1)}(x_2 = 0) = \tau_{23}^{(2)}(x_2 = 0) \tag{18}$$

Substituting Eqs. 13 and 14 into boundary conditions, Eqs. 17 and 18, one obtains two linear homogeneous algebraic equations for two unknown amplitude coefficients C_1 and C_2, namely:

$$C_1 = C_2 \tag{19}$$

$$C_1 \frac{q_1}{s_{44}^{(1)}(\omega)} = -C_2 \frac{q_2}{s_{44}^{(2)}} \tag{20}$$

Combining Eqs. 19 and 20, we get the following dispersion equation for the new SH elastic surface waves:

$$\frac{q_1}{-s_{44}^{(1)}(\omega)} = \frac{q_2}{s_{44}^{(2)}} \tag{21}$$

The sign "−" before the compliance $-s_{44}^{(1)}(\omega)$ plays a crucial role in the analysis of new SH elastic surface waves, since it implies that if the transverse wavenumbers q_1 and q_2 are positive, the elastic compliances $s_{44}^{(1)}(\omega)$, $s_{44}^{(2)}$ must be of the opposite sign $s_{44}^{(1)}(\omega) \cdot s_{44}^{(2)} < 0$. Consequently, if the elastic compliance $s_{44}^{(1)}(\omega)$ (see Eq.1) in the metamaterial half-space is negative for $\omega < \omega_p$, the compliance $s_{44}^{(2)}$ have to be positive (see Fig.1).

Since $C_1 = C_2$ (see Eq.19) in the following of this paper we will use only one amplitude coefficient, denoted as $C = C_1 = C_2$.

3.3 Wavenumber $k(\omega)$

Substituting Eq.16, for transverse wavenumbers q_1 and q_2, in the dispersion relation Eq.21 one obtains the following formula for the wavenumber $k(\omega)$ of the new SH elastic surface wave

$$k(\omega) = k_2 \sqrt{\frac{s_{44}^{(1)}(\omega)}{s_{44}^{(1)}(\omega) + s_{44}^{(2)}}} \sqrt{\frac{s_{44}^{(2)} \frac{\rho_1}{\rho_2} - s_{44}^{(1)}(\omega)}{s_{44}^{(2)} - s_{44}^{(1)}(\omega)}} \tag{22}$$

where: the wavenumber of bulk SH waves in the conventional elastic half-space $k_2 = \omega\sqrt{s_{44}^{(2)}\rho_2}$.

Since the wavenumber $k(\omega)$ of the new SH elastic surface wave has to be real and positive, Eq.22 imposes the following two necessary conditions on $s_{44}^{(1)}(\omega)$ and $s_{44}^{(2)}$

$$\left(s_{44}^{(1)}(\omega) < 0\right) and \left(s_{44}^{(1)}(\omega) + s_{44}^{(2)}\right) < 0 \tag{23}$$

The first condition requires that $\omega < \omega_p$ and the second gives rise to $\omega < \omega_{sp}$, where the cut-off angular frequency ω_{sp} and the angular frequency of local resonances ω_p are related by:

$$\omega_{sp} = \omega_p \Big/ \sqrt{\frac{s_{44}^{(2)}}{s_0} + 1} \tag{24}$$

Since ω_p is always higher than ω_{sp} ($\omega_p > \omega_{sp}$), the two conditions given by Eq.23 imply that the frequency ω of the new SH elastic surface wave has to be limited to the range $0 < \omega < \omega_{sp}$.

In the context of the SPP electromagnetic surface waves the angular frequency ω_{sp} is called the surface plasmon resonance frequency [17].

3.4 Phase velocity $v_p(\omega)$

Since by definition $k(\omega) = \omega / v_p\,(\omega)$, the analytical formula for the phase velocity $v_p(\omega)$ of new SH elastic surface waves results immediately from Eq.22:

$$v_p(\omega) = v_2 \sqrt{\frac{s_{44}^{(1)}(\omega) + s_{44}^{(2)}}{s_{44}^{(1)}(\omega)}} \sqrt{\frac{s_{44}^{(2)} - s_{44}^{(1)}(\omega)}{s_{44}^{(2)} \frac{\rho_1}{\rho_2} - s_{44}^{(1)}(\omega)}} \tag{25}$$

where: $v_2 = 1 \Big/ \sqrt{s_{44}^{(2)} \rho_2}$ is the phase velocity of bulk SH waves in the conventional elastic half-space.

3.5 Group velocity $v_g(\omega)$

Differentiation of Eq.22 for the wavenumber $k(\omega)$, with respect to the angular frequency ω, leads to the following formula for the group velocity $v_g(\omega) = d\omega / dk$ of the new SH surface wave:

$$\frac{v_g(\omega)}{v_2} \frac{v_p(\omega)}{v_2} = \frac{\left[\left[s_{44}^{(2)}\right]^2 - \left[s_{44}^{(1)}(\omega)\right]^2\right]^2}{s_{44}^{(1)}(\omega)\left[\frac{\rho_1}{\rho_2} s_{44}^{(2)} - s_{44}^{(1)}(\omega)\right]\left[\left[s_{44}^{(2)}\right]^2 - \left[s_{44}^{(1)}(\omega)\right]^2\right] + \frac{\omega}{2} \frac{d s_{44}^{(1)}(\omega)}{d\omega}\left[\frac{\rho_1}{\rho_2}\left[\left[s_{44}^{(2)}\right]^2 + \left[s_{44}^{(1)}(\omega)\right]^2\right] - 2 s_{44}^{(1)}(\omega) s_{44}^{(2)}\right]} \tag{26}$$

Despite its relative complexity, Eq.26 is quite elementary and can be easily implemented in numerical calculations.

3.6 Penetration depths $\delta_1(\omega), \delta_2(\omega)$ in both half-spaces of the waveguide

The penetration depth in t-he metamaterial half-space $x_2 < 0$ is defined as $\delta_1(\omega) = 1/q_1(\omega)$, where the transverse wave number $q_1(\omega) = \sqrt{k^2 - k_1^2}$ (see Eq.16) and $k_1^2 = \omega^2 s_{44}^{(1)}(\omega)\rho_1$. Similarly, in the conventional elastic half-space $x_2 \geq 0$ we have $\delta_2(\omega) = 1/q_2(\omega)$, where the transverse wavenumber $q_2(\omega) = \sqrt{k^2 - k_2^2}$ (see Eq.16) and $k_2^2 = \omega^2 s_{44}^{(2)}\rho_2$.

Consequently, substituting Eq.22 for the wavenumber k into Eq.16 for the transverse wavenumbers q_1 and q_2 and noting that $\lambda = 2\pi/k$ one obtains:

$$\delta_1(\omega) = \frac{\lambda}{2\pi}\sqrt{\frac{s_{44}^{(2)}\left[-s_{44}^{(1)}(\omega) + s_{44}^{(2)}\frac{\rho_1}{\rho_2}\right]}{-s_{44}^{(1)}(\omega)\left[s_{44}^{(2)} - s_{44}^{(1)}(\omega)\frac{\rho_1}{\rho_2}\right]}} \tag{27}$$

$$\delta_2(\omega) = \frac{\lambda}{2\pi}\sqrt{\frac{-s_{44}^{(1)}(\omega)\left[-s_{44}^{(1)}(\omega) + s_{44}^{(2)}\frac{\rho_1}{\rho_2}\right]}{s_{44}^{(2)}\left[s_{44}^{(2)} - s_{44}^{(1)}(\omega)\frac{\rho_1}{\rho_2}\right]}} \tag{28}$$

where λ is the wavelength of the new SH elastic surface wave.

In general, the ratio of the penetration depths $\delta_1(\omega)$, $\delta_2(\omega)$ is expressed by the dispersion equation (Eq.21), i.e., $\delta_2(\omega)/\delta_1(\omega) = -s_{44}^{(1)}(\omega)/s_{44}^{(2)}$ that is independent on ρ_1/ρ_2. On the other hand, by virtue of Eqs. 27 and 28 the product of the normalized penetration depths equals:

$$\frac{\delta_1(\omega)}{\lambda}\cdot\frac{\delta_2(\omega)}{\lambda} = \left(\frac{1}{2\pi}\right)^2 \frac{-s_{44}^{(1)}(\omega) + s_{44}^{(2)}\frac{\rho_1}{\rho_2}}{s_{44}^{(2)} - s_{44}^{(1)}(\omega)\frac{\rho_1}{\rho_2}} \tag{29}$$

However, if the density in both half-spaces of the waveguide is the same ($\rho_1 = \rho_2$) then Eq. 29 reduces to

$$\frac{\delta_1(\omega)}{\lambda}\cdot\frac{\delta_2(\omega)}{\lambda} = \left(\frac{1}{2\pi}\right)^2 \tag{30}$$

Thus, if the density in both half-spaces of the waveguide is identical ($\rho_1 = \rho_2$) the product of the normalized penetration depths $\delta_1(\omega)\delta_2(\omega)/\lambda^2$ is independent of angular frequency ω and material constants of the waveguide and equals $(1/2\pi)^2 \approx 0.025$. In other words, if $\rho_1 = \rho_2$ both normalized penetration depths $\delta_1(\omega)/\lambda$, $\delta_2(\omega)/\lambda$ are inversely proportional. As a result, if $\delta_1(\omega)/\lambda$ increases then $\delta_2(\omega)/\lambda$ decreases accordingly to Eq.30 and vice-versa. Simultaneously, if the angular

frequency $\omega \to \omega_{sp}$ then both $\delta_1(\omega)/\lambda$ and $\delta_2(\omega)/\lambda$ are subwavelength and tend to the same value $1/2\pi$ (see Figs 11 and 12).

3.7 Active power flow $P_1^{(1)}(\omega), P_1^{(2)}(\omega)$ in the direction of propagation x_1

The complex Poynting vector $P_1^{(i)}(x_2)$, in the direction of propagation x_1, of new SH elastic surface waves can be expressed as $P_1^{(i)}(x_2) = -\frac{1}{2}\left[\tau_{13}^{(i)}(x_2) \cdot \left(-j\omega u_3^{(i)}(x_2)\right)^*\right]$, where $u_3^{(i)}(x_2)$ is the mechanical displacement (Eq.5) and $\tau_{13}^{(i)}(x_2)$ is the mechanical stress (Eq.15), where $i = 1,2$.

Similarly, the complex power flow (per unit length along the axis x_3) in the metamaterial half-space ($x_2 < 0$) is defined as $P_1^{(1)}(\omega) = \int_{-\infty}^{0} P_1^{(1)}(x_2)dx_2$ (see Fig.1) and in the conventional elastic half-space ($x_2 \geq 0$) by $P_1^{(2)}(\omega) = \int_0^{\infty} P_1^{(2)}(x_2)dx_2$.

Consequently, using Eqs. 13 and 15 it can be shown that the complex power flows $P_1^{(1)}(\omega)$ and $P_1^{(2)}(\omega)$ in both half-spaces of the waveguide are given by:

$$P_1^{(1)}(\omega) = -\frac{1}{4}|C|^2 \frac{k(\omega)\omega}{-s_{44}^{(1)}(\omega)q_1(\omega)} \tag{31}$$

$$P_1^{(2)}(\omega) = \frac{1}{4}|C|^2 \frac{k(\omega)\omega}{s_{44}^{(2)}q_2(\omega)} \tag{32}$$

where C is an arbitrary amplitude coefficient.

It should be noticed that all field variables entering Eqs. 31, 32 are real. Therefore, the power flows $P_1^{(1)}(\omega)$ and $P_1^{(2)}(\omega)$ in both half-spaces of the waveguide are active. In other words, new SH elastic surface waves can transfer effectively the active power along the guiding interface $x_2 = 0$ in the direction of propagation x_1.

Employing the dispersion Eq. 21 in conjunction with Eqs. 31, 32 the ratio of the active powers flows $P_1^{(1)}(\omega)/P_1^{(2)}(\omega)$ in both half-spaces of the waveguide is given by

$$\frac{P_1^{(1)}(\omega)}{P_1^{(2)}(\omega)} = \frac{s_{44}^{(2)}}{s_{44}^{(1)}(\omega)}\frac{q_2(\omega)}{q_1(\omega)} = -\left[\frac{\delta_1(\omega)}{\delta_2(\omega)}\right]^2 \tag{33}$$

Note that the ratio of the active power flows in both half-spaces is always negative, since $s_{44}^{(1)}(\omega)$ and $s_{44}^{(2)}$ are of the opposite sign and the transverse wavenumbers are real and positive $q_1(\omega)$, $q_2(\omega) > 0$. Consequently, $P_1^{(1)}(\omega)$ and $P_1^{(2)}(\omega)$ propagate in opposite directions along axis x_1.

3.8 Reactive power flow $P_2^{(1)}(\omega), P_2^{(2)}(\omega)$ in the transverse direction x_2

The complex Poynting vector $P_2^{(i)}(x_2)$, in the transverse direction x_2, of new SH elastic surface waves can be expressed as $P_2^{(i)}(x_2) = -\frac{1}{2}\left[\tau_{23}^{(i)}(x_2) \cdot \left(-j\omega u_3^{(i)}(x_2)\right)^*\right]$, where $u_3^{(i)}(x_2)$ is the mechanical displacement (Eq.13) and $\tau_{23}^{(i)}(x_2)$ is the mechanical stress (Eq.14), where $i = 1,2$.

Similarly, the complex power flow (per unit length along the axis x_3) in the metamaterial half-space ($x_2 < 0$) is defined as $P_2^{(1)}(\omega) = \int_{-\infty}^{0} P_2^{(1)}(x_2)dx_2$ (see Fig.1) and in the conventional elastic half-space ($x_2 \geq 0$) by $P_2^{(2)}(\omega) = \int_0^{\infty} P_2^{(2)}(x_2)dx_2$.

Consequently, using Eqs. 13 and 14 it can be shown that the complex power flow $P_2^{(1)}(\omega)$ and $P_2^{(2)}(\omega)$ in both half-spaces are given by:

$$P_2^{(1)}(\omega) = +j\frac{\omega}{4}|C|^2\frac{1}{-s_{44}^{(1)}(\omega)} \tag{34}$$

$$P_2^{(2)}(\omega) = +j\frac{\omega}{4}|C|^2\frac{1}{s_{44}^{(2)}} \tag{35}$$

Thus, if $\omega \to 0$ then $P_2^{(1)}(\omega)$ and $P_2^{(2)}(\omega)$ both tend to zero. On the other hand, if $\omega \to \omega_{sp}$ then $P_2^{(2)}(\omega)$ and $P_2^{(1)}(\omega)$ tend to the same value, namely $j(\omega_{sp}/4)|C|^2/s_{44}^{(2)}$.

Since the elastic compliance $s_{44}^{(1)}(\omega)$ is negative, in the frequency range $0 < \omega < \omega_{sp}$, the reactive power flows $P_2^{(1)}(\omega), P_2^{(2)}(\omega)$, in both half-spaces, are both positive (+) and correspond to the inductive type of the reactive power, in analogy to SPP electromagnetic waves.

Using Eq.1 together with Eqs. 34 and 35, the ratio of the reactive power flows in both half-spaces can be written as:

$$\frac{P_2^{(1)}(\omega)}{P_2^{(2)}(\omega)} = -\frac{s_{44}^{(2)}}{s_{44}^{(1)}(\omega)} = \frac{\delta_1(\omega)}{\delta_2(\omega)} \tag{36}$$

Comparing Eqs. 33 and 36 one obtains rather unexpected relation between the active power flows $P_1^{(1)}(\omega), P_1^{(2)}(\omega)$ in the direction of propagation x_1 and the reactive power flows $P_2^{(1)}(\omega), P_2^{(2)}(\omega)$ in the transverse direction x_2, namely:

$$\frac{P_1^{(1)}(\omega)}{P_1^{(2)}(\omega)} = -\left[\frac{P_2^{(1)}(\omega)}{P_2^{(2)}(\omega)}\right]^2 \tag{37}$$

Thus, if the ratio of the active power flows $P_1^{(1)}(\omega)/P_1^{(2)}(\omega)$ increases, say 4 times, the ratio of the reactive power flow $P_2^{(1)}(\omega)/P_2^{(2)}(\omega)$ grows only 2 times, etc. In other words, repartition of the active power flow $(P_1^{(1)}(\omega), P_1^{(2)}(\omega))$ between two half-spaces of the waveguide is much more sensitive to changes in the penetration depths $\delta_1(\omega)/\lambda$ and $\delta_2(\omega)/\lambda$ than that of the reactive power flow $(P_2^{(1)}(\omega), P_2^{(2)}(\omega))$ in the transverse direction x_2.

4. Correspondence between the SPP electromagnetic waves and the proposed new SH elastic surface waves

As it was stated before, the proposed new SH surface acoustic waves can be considered as an elastic analogue of SPP electromagnetic surface waves propagating in metal-dielectric interface. In fact, the mathematical models of both types of waves exhibit strong similarities. Therefore it will be advantageous to identify explicitly the corresponding field variables in both domains, since the results obtained in one domain can be directly transferred to the other domain, alleviating thereby tedious from scratch derivations of the resulting analytical formulas (see Table 1).

~~Some caution however has to be observed, since a number of notions commonly used in electromagnetism do not have direct counterparts in the theory of elasticity. For example, in the electromagnetic domain one uses very often the notion of the relative material constants, such as the relative dielectric permittivity or relative magnetic permeability. By contrast, in the theory of elasticity the use of the relative material constants was not adopted mainly due to the fact that such a universally accepted reference medium as vacuum does not exist. Similarly, the notion of the index of refraction, commonly used in electromagnetism, did not gain much popularity in the theory of elasticity for the same reason.~~

Table 1 Correspondence between field variables of SPP electromagnetic waves in metal-dielectric waveguides and the proposed new SH elastic surface waves in metamaterial waveguides

No	SPP electromagnetic surface waves in metal-dielectric waveguides		New SH elastic surface waves in metamaterial waveguides	
	Property	Implementation	Implementation	Property
1	Longitudinal electric field	E_1	τ_{23}	Shear horizontal SH mechanical stress
2	Transverse electric field	E_2	τ_{13}	Shear mechanical stress
3	transverse magnetic field	H_3	$v_3 = -j\omega u_3$	SH particle velocity $v_3 = \partial u_3/\partial t$
4	Dielectric function in metal	$\varepsilon_1(\omega)$	$s_{44}^{(1)}(\omega)$	Elastic compliance in metamaterial half-space
5	Dielectric function in dielectric	ε_2	$s_{44}^{(2)}$	Elastic compliance in conventional half-space
6	Magnetic permeability in metal	μ_1	ρ_1	Density of metamaterial half-space
7	Magnetic permeability in dielectric	μ_2	ρ_2	Density of conventional half-space

8	Wavenumber for $\mu_1/\mu_2 = 1$	$k(\omega) = k_2\sqrt{\frac{\varepsilon_1(\omega)}{\varepsilon_1(\omega)+\varepsilon_2}}$	$k(\omega) = k_2\sqrt{\frac{s_{44}^{(1)}(\omega)}{s_{44}^{(1)}(\omega)+s_{44}^{(2)}}}$	Wavenumber for $\rho_1/\rho_2 = 1$
9	Phase velocity of SPP electromagnetic waves	$v_p(\omega) = v_2\sqrt{\frac{\varepsilon_1(\omega)+\varepsilon_2}{\varepsilon_1(\omega)}}$	$v_p(\omega) = v_2\sqrt{\frac{s_{44}^{(1)}(\omega)+s_{44}^{(2)}}{s_{44}^{(1)}(\omega)}}$	Phase velocity of new SH elastic surface waves
10	Complex Poynting vector in propagation direction x_1	$P_1 = \frac{1}{2}E_2 \times H_3^*$	$P_1 = -\frac{1}{2}\tau_{13}v_3^*$	Complex Poynting vector in propagation direction x_1
11	Complex Poynting vector in transverse direction x_2	$P_2 = \frac{1}{2}E_1 \times H_3^*$	$P_2 = -\frac{1}{2}\tau_{23}v_3^*$	Complex Poynting vector in transverse direction x_2
12	Wave impedance $Z_{TM} = E_2/H_3$, TM modes	$Z_{TM}^{-1} = v_p(\omega)\begin{cases}\varepsilon_1(\omega), metal\\ \varepsilon_2, dielec\end{cases}$	$Z_s^{-1} = v_p(\omega)\begin{cases}s_{44}^{(1)}(\omega), meta.\\ s_{44}^{(2)}, conven.\end{cases}$	Wave impedance $Z_s = -\tau_{13}/v_3$,elastic surface waves

5. Results

5.1 Dispersion curves

Figure 8 presents the dispersion curves of the new surface acoustic wave. Using Eq.22 one can show that if $\omega \to 0$ then $k(\omega) \to 0$. On the other hand, when $\omega \to \omega_{sp}$ then the wavenumber $k(\omega) \to \infty$, (see Fig.8).

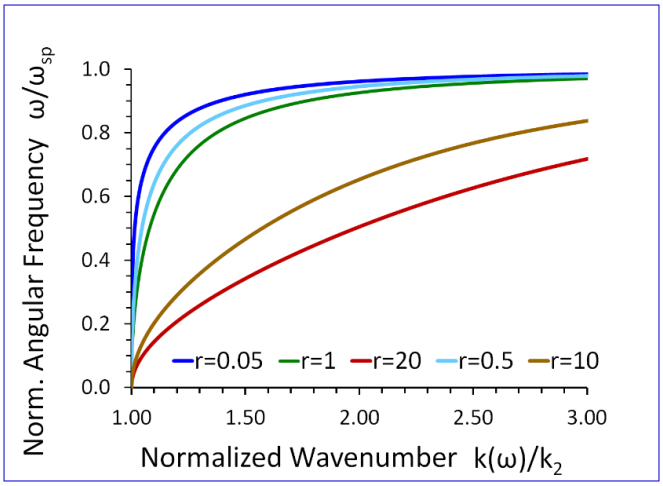

Fig.8 Normalized angular frequency ω/ω_{sp} versus normalized wavenumber $k(\omega)/k_2$, for $r = \rho_1/\rho_2$ as a parameter ($s_{44}^{(2)}/s_0 = 1$).

5.2. Phase velocity

Eq.25 shows that if $\omega \to 0$ then $v_p(\omega) \to v_2$. On the other hand, when $\omega \to \omega_{sp}$ then the phase velocity $v_p(\omega) \to 0$, (see Fig.9).

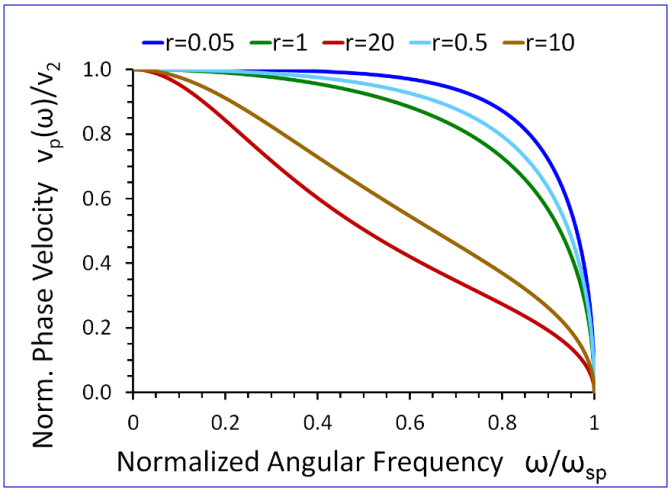

Fig.9 Normalized phase velocity $v_p(\omega)/v_2$ versus normalized angular frequency ω/ω_{sp}, for $r = \rho_1/\rho_2$ as a parameter ($s_{44}^{(2)}/s_0 = 1$)

5.3. Group velocity

Closer look at Eq.26 reveals that if $\omega \to 0$ then $v_g(\omega) \to v_2$ (see Fig.10. On the other hand, when $\omega \to \omega_{sp}$ then $v_g(\omega) \to 0$. Thus, phase $v_p(\omega)$ and group $v_g(\omega)$ velocities tend to the same limiting values for $\omega \to 0$ and $\omega \to \omega_{sp}$, (see Figs 9 and 10).

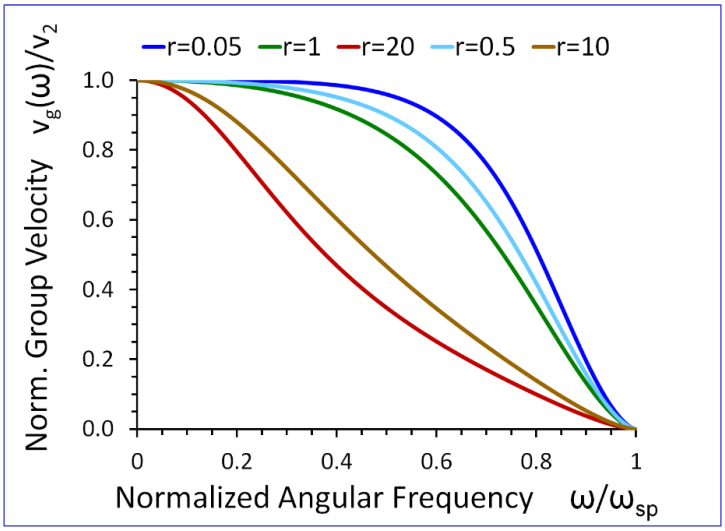

Fig.10 Normalized group velocity $v_g(\omega)/v_2$ versus normalized angular frequency ω/ω_{sp}, for $r = \rho_1/\rho_2$ as a parameter ($s_{44}^{(2)}/s_0 = 1$)

5.4. Penetration depths in both half-spaces

Equation 27 shows that If the angular frequency $\omega \to 0$ then the normalized penetration depth in the metamaterial half-space $\delta_1(\omega)/\lambda \to 0$. On the other hand, when $\omega \to \omega_{sp}$ then $\delta_1(\omega)/\lambda \to 1/2\pi$. Thus, the normalized penetration depth $\delta_1(\omega)/\lambda$ in the metamaterial half-space is always subwavelength, i.e., $\delta_1(\omega)/\lambda < 1/2\pi$, (see Fig.11).

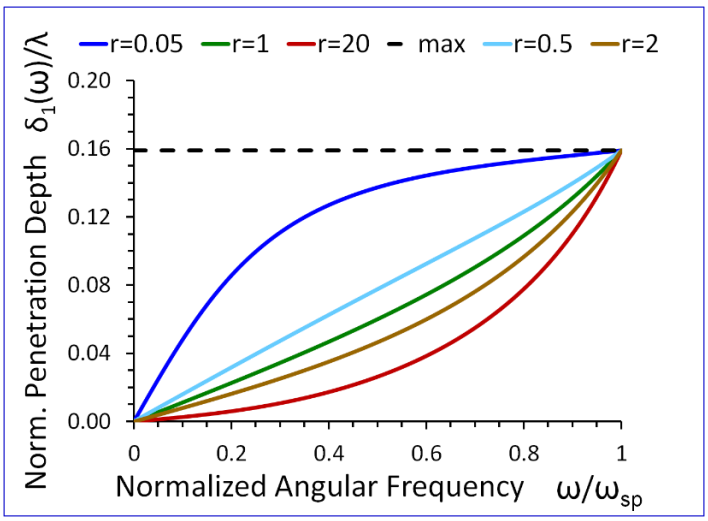

Fig.11 Normalized penetration depth $\delta_1(\omega)\ /\lambda$ in the metamaterial half-space, versus normalized angular frequency ω/ω_{sp}, for $r = \rho_1/\rho_2$ as a parameter $(s_{44}^{(2)}/s_0 = 1)$.

On the other hand (see Eq.28), the normalized penetration depth in the conventional elastic half-space $\delta_2(\omega)/\lambda \to \infty$, if angular frequency $\omega \to 0$. Similarly, when $\omega \to \omega_{sp}$ then $\delta_2(\omega)/\lambda \to 1/2\pi$. As a result, the normalized penetration depth $\delta_2(\omega)/\lambda$ is higher than "1" (see dotted horizontal line in Fig.12) for low frequencies and subwavelength for high frequencies approaching the cut-off frequency ω_{sp}, (see Fig.12).

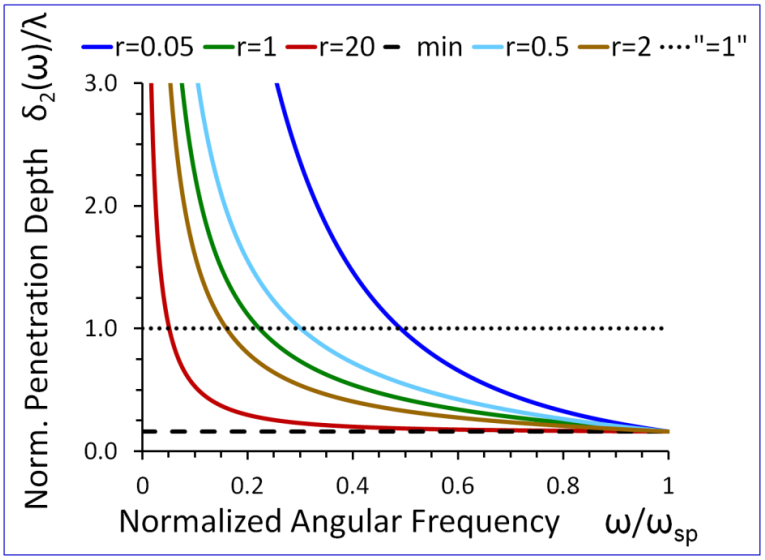

Fig.12 Normalized penetration depth $\delta_2(\omega)\ /\lambda$ in the conventional elastic half-space, versus normalized angular frequency ω/ω_{sp}, for $r = \rho_1/\rho_2$ as a parameter $(s_{44}^{(2)}/s_0 = 1)$.

5.5. Active power flow in the direction of propagation x_1

Using Eq.33 in conjunction with Eqs. 27 and 28 one can show that if $\omega \to 0$ then $P_1^{(1)}(\omega)/P_1^{(2)}(\omega) \to 0$. On the other hand, if $\omega \to \omega_{sp}$ then $P_1^{(1)}(\omega)/P_1^{(2)}(\omega) \to -1$, (see Fig.13).

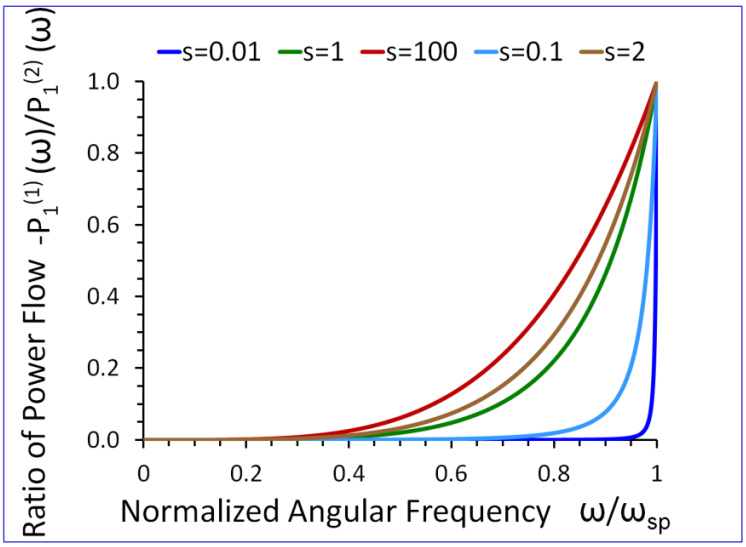

Fig.13 Ratio of active power flows $-P_1^{(1)}(\omega)/P_1^{(2)}(\omega)$, in the direction of propagation x_1, versus normalized angular frequency ω/ω_{sp}, for $s = s_{44}^{(2)}/s_0$ as a parameter. ρ_1 and ρ_2 are arbitrary.

5.6. Reactive power flow in the transverse direction x_2

From Eq. 36 we can conclude that if $\omega \to 0$ then $P_2^{(1)}(\omega)/P_2^{(2)}(\omega)$ tends to zero. On the other hand, if $\omega \to \omega_{sp}$ then $P_2^{(1)}(\omega)/P_2^{(2)}(\omega) \to 1$, (see Fig.14).

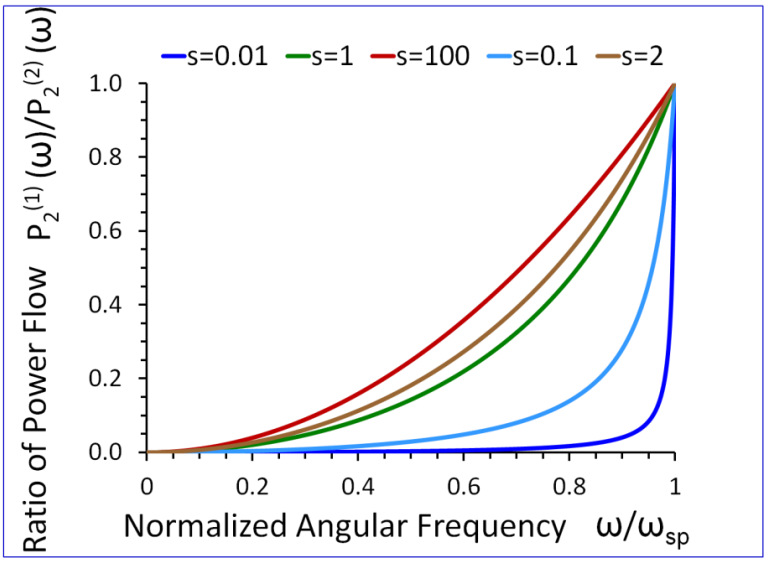

Fig.14 Ratio of reactive power flows $P_2^{(1)}(\omega)/P_2^{(2)}(\omega)$, in the transverse direction x_2, versus normalized angular frequency ω/ω_{sp}, for $s = s_{44}^{(2)}/s_0$ as a parameter. ρ_1 and ρ_2 are arbitrary.

6. Discussion

Acoustic surface waves propagating in metamaterial waveguides were subject of a number of papers that analyzed Rayleigh surface waves at the solid-vacuum interface [20], Scholte interfacial waves at the solid-liquid interface [21], shear horizontal waves on a semi-infinite half-space loaded with a metasurface [22, 23] and Love surface waves in waveguides loaded with a metasurface [24]. However, to the best of our knowledge SH elastic surface waves propagating at the interface between two elastic half-spaces, one of which is an elastic metamaterial, were yet analyzed in the scientific literature.

Our former research [25] on elastic surface waves propagating in conventional elastic waveguides showed that SH surface waves, such as Love surface waves [26], share many common properties with waves in other domains of physics, such as TM (Transverse Magnetic) modes in optical planar waveguides or wave function of quantum particles in a potential well. However, the present paper was mostly influenced by recent developments in the domain of elastic metamaterials and SPP electromagnetic surface waves propagating at the metal-dielectric interface [27].

In this paper we demonstrated that the ultrasonic analogue of SPP electromagnetic waves can exist in layered elastic waveguides consisting of 2 elastic half-spaces, providing that one of the elastic half-spaces is an elastic metamaterial with a negative elastic compliance $s_{44}^{(1)}(\omega)$ that corresponds to the dielectric function $\varepsilon(\omega)$ in Drude's model of metals. These two types of waves have similar: 1) distribution of wave fields, 2) dispersion equations etc.

The dispersion curves of the new ultrasonic wave shown in Fig.8 have the characteristic property that the wavenumber $k(\omega)$ tends to infinity $k(\omega) \to \infty$, when the wave angular frequency ω approaches cuff-of angular frequency ω_{sp}. This means that the wavelength λ of the new ultrasonic surface wave tends to zero $\lambda \to 0$ when $\omega \to \omega_{sp}$, what can be employed in the subwavelenght near field acoustic imaging.

A very intriguing property of the new SH ultrasonic waves is that they slow down, i.e., the phase $v_p(\omega)$ and group $v_g(\omega)$ velocities tend to zero as the wave frequency approaches the cut-off frequency $\omega \to \omega_{sp}$ (see Figs. 9 and 10). This property is crucial in potential applications of the new SH ultrasonic wave in ultrasonic sensors with extremely large mass sensitivity.

This paper contains a number of new original formulas, that to the best of our knowledge, were not yet published in the literature, namely:

- relation for the product of penetration depths $\delta_1(\omega)$, $\delta_2(\omega)$ in two half-spaces of the waveguide (Eq.30)

- relation between active power flows $P_1^{(1)}(\omega)$, $P_1^{(2)}(\omega)$ in the direction of propagation x_1 and penetration depths $\delta_1(\omega)$, $\delta_2(\omega)$ in two half-spaces of the waveguide (Eq.33)
- relation between reactive power flows $P_2^{(1)}(\omega)$, $P_2^{(2)}(\omega)$ in the transverse direction x_2 and penetration depths $\delta_1(\omega)$, $\delta_2(\omega)$ in two half-spaces of the waveguide (Eq.36)
- relation between active power flows $P_1^{(1)}(\omega)$, $P_1^{(2)}(\omega)$ in the direction of propagation x_1 and reactive power flows $P_2^{(1)}(\omega)$, $P_2^{(2)}(\omega)$ in the transverse direction x_2 of the waveguide (Eq.37)

All new equations mentioned above in the mechanical domain can be directly transferred into the domain of SPP electromagnetic surface waves, using to this end Table 1 presented in Section 4. In particular, the relation between the penetration depths $\delta_1(\omega)$, $\delta_2(\omega)$ in two half-spaces of the waveguide (Eq.30) can be useful for designers of SPP electromagnetic sensors, in selection of proper wave frequency providing high subwavelength concentration of energy in the dielectric material of the waveguide leading to long range propagation of SPP waves.

Similarly, the new relations between the power flows and the penetration depths in two half-spaces of the waveguide (Eqs. 33 and 36) indicate that the proper control of the active power flow in the direction of propagation may be very important in achieving high sensitivity of long range SPP sensors with low losses.

The results presented in Figs. 8-12 reveal that the densities ρ_1, ρ_2, in both half-spaces of the waveguide, have a profound impact on all parameters of the proposed new elastic surface waves. For example, if $\rho_1/\rho_2 = 1$, the penetration depth in the metamaterial half-space $\delta_1(\omega)$ is ~43 times smaller than the wavelength λ of the wave, at $\omega/\omega_{sp} = 0.2$ (see green curve Fig.11). By contrast, if $\rho_1/\rho_2 = 20$ the penetration depth $\delta_1(\omega)$ decreases significantly and is ~167 times smaller than the wavelength λ (see red curve in Fig.11).

Therefore, since ρ_1, ρ_2 correspond to magnetic permeabilities μ_1, μ_2 in SPP electromagnetic waveguides (see Table 1 in Section 4) it implies that we can also effectively shape the characteristics of SPP electromagnetic waves by analogous adjustment of μ_1 and μ_2.

On the other hand, due to strong formal similarities between the new SH acoustic surface waves and SPP electromagnetic surface waves it may be possible in future to transfer newly discovered SPP phenomena, such as cloaking [14], trapping (zero group velocity) [13] and topological protection [15] into the domain of elastic metamaterials using to this end the new SH elastic surface waves, proposed in this paper.

Thus, the proposed new SH acoustic surface waves open new possibilities to control wave phenomena in elastic solids and can constitute the basis for a new generation of modern devices in the domain of microwave acoustics.

As a result, this paper is an example of multidisciplinary research that can shed new valuable and sometimes unexpected physical insight on physical phenomena occurring in two domains of physics, i.e., theory of elasticity and electromagnetism.

It will be advantageous in future research to extend the analysis of the new SH elastic surface waves on waveguides with losses as well as to design a model of a biosensor based on the analogy with SPP electromagnetic devices [28, 29].

7. Conclusions

Based on the results of research presented in this paper, we can draw the following conclusions:

1. The new SH elastic surface waves can be considered as an elastic analogue of the electromagnetic SPP waves, due to strong formal similarities of their mathematical models (Table 1 in Section 4).

2. The new SH elastic surface waves can exist at the interface of two elastic half-spaces one of which is an elastic metamaterial with a negative compliance $s_{44}^{(1)}(\omega) \cdot s_{44}^{(2)} < 0$ (Eq.21).

3. Phase velocity $v_p(\omega)$ of the new SH ultrasonic surface waves is antiparallel to the active power flow $P_1^{(1)}(\omega)$ in the metamaterial half-space and parallel to the active power flow $P_1^{(2)}(\omega)$ in the conventional elastic half-space.

4. Active power flows $P_1^{(1)}(\omega), P_1^{(2)}(\omega)$ of the new SH elastic surface waves, in both half-spaces, are antiparallel along the direction of propagation x_1, (Eqs. 31 and 32).

5. Reactive power flows $P_2^{(1)}(\omega), P_2^{(2)}(\omega)$, in the transverse direction x_2, have the same sign (+) corresponding to the inductive type of the reactive power, oscillating between two half-spaces of the waveguide (Eqs. 34 and 35).

6. The penetration depth $\delta_1(\omega)$ of the new SH elastic surface waves in the metamaterial half-space is always smaller than that in the conventional elastic half-space $\delta_2(\omega)$, i.e., $\delta_1(\omega) < \delta_2(\omega)$ (Figs. 11 and 12).

7. The ratio of the active power flows $P_1^{(1)}(\omega)/P_1^{(2)}(\omega)$ and the corresponding ratio of the reactive power flows $P_2^{(1)}(\omega)/P_2^{(2)}(\omega)$ are intimately related to the ratio of the penetration depths $\delta_1(\omega)/\delta_2(\omega)$ in both half-spaces of the waveguide (Eqs. 33, 36 and Figs. 13-14).

8. The ratio of the active power flows $P_1^{(1)}(\omega)/P_1^{(2)}(\omega)$ and the corresponding ratio of the reactive power flows $P_2^{(1)}(\omega)/P_2^{(2)}(\omega)$ are not independent since they are related via Eq.37.

9. The penetration depth (see Figs. 11 and 12) in both elastic half-spaces of the waveguide is deeply subwavelength. Therefore, the new SH elastic surface waves can find applications in sensors of extremely high mass sensitivity,

superlensing and in near field acoustic microscopy with a subwavelength resolution and imaging. These are very exciting applications of the newly discovered SH ultrasonic waves.

10. A number of new formulas (Eqs. 30, 33, 36 and 37) developed in this paper may be useful in design of long range SPP waveguides with low propagation losses.

11. The densities ρ_1, ρ_2, in both half-spaces of the waveguide, have a profound impact on all parameters of the proposed new elastic surface waves (Figs 8-12). Therefore, by virtue of Table 1 in Section 4 we can also effectively shape the characteristics of SPP electromagnetic waves by analogous adjustment of the corresponding magnetic permeabilities μ_1 and μ_2.

12. Newly discovered SPP phenomena, such as cloaking, trapping (zero group velocity) and topological protection can be transferred into the domain of elastic metamaterials using to this end the new SH elastic surface waves, proposed in this paper. This is a novelty.

The proposed, in this paper, new SH ultrasonic surface wave could play a key role in achieving subwavelength acoustic imaging, enhanced transmission, slow wave effects and superlensing below the diffraction limit.

Because of its interdisciplinary character, this paper can be of interest for a broad spectrum of researchers working in different domains of physics such as: acoustics, ultrasonics, elastodynamics, metamaterials, electromagnetism and optics.

Acknowledgement: The project was funded by the National Science Centre (Poland), granted on the basis of Decision No 2020/39/B/ST8/03505

References

[1] M. Kadic, T. Bückmann, R. Schittny and M. Wegener, Metamaterials beyond electromagnetism, Reports on Progress in Physics, 76, 126501 (34pp), (2013), https://doi.org/10.1088/0034-4885/76/12/126501

[2] Romain Fleury, Francesco Monticone, and Andrea Alù, Invisibility and Cloaking: Origins, Present, and Future Perspectives, PHYSICAL REVIEW APPLIED 4, 037001 (2015) https://doi.org/10.1103/PhysRevApplied.4.037001

[3] Kenny L. S. Yip and Sajeev John, Acoustic modes of locally resonant phononic crystals: Comparison with frequency-dependent mass models, PHYSICAL REVIEW B 103, 094304 (2021), https://doi.org/10.1103/PhysRevB.103.094304

[4] Rogelio Graciá-Salgado, Victor M. García-Chocano, Daniel Torrent, and José Sánchez-Dehesa, Negative mass density and ρ-near-zero quasi-two-dimensional metamaterials: Design and applications, Phys. Rev. B 88, 224305 (2013) https://doi.org/10.1103/PhysRevB.88.224305

[5] Wei Wang, Bernard Bonello, Bahram Djafari-Rouhani, Yan Pennec, and Jinfeng Zhao, Double-Negative Pillared Elastic Metamaterial, Phys. Rev. Applied 10, 064011 (2018), https://doi.org/10.1103/PhysRevApplied.10.064011

[6] Daniel Torrent, Yan Pennec, and Bahram Djafari-Rouhani, Resonant and nonlocal properties of phononic metasolids, Phys. Rev. B 92, 174110 (2015) https://doi.org/10.1103/PhysRevB.92.174110

[7] Y. Wu, Y. Lai, and Z-Q Zhang, Elastic metamaterials with simultaneously negative effective shear modulus and mass density, Physical Review Letters, 107, 105506, (2011) https://doi.org/10.1103/PhysRevLett.107.105506

[8] Xiaoming Zhou, Xiaoning Liu and Gengkai Hu, Elastic metamaterials with local resonances: an overview, THEORETICAL & APPLIED MECHANICS LETTERS **2**, 041001 (2012), https://doi.org/10.1063/2.1204101

[9] J.D. Achenbach, Wave Propagation in Elastic Solids, North-Holland, Amsterdam (1973)

[10] J. Zhang, L. Zhang and W. Xu, Surface plasmon polaritons: physics and applications, Topical Review, Journal of Physics D: Applied Physics, 45, 113001 (19pp), (2012) https://doi.org/10.1088/0022-3727/45/11/113001

[11] S.A. Maier, Plasmonics: Fundamentals and Applications, Springer, 2007

[12] I.R.Hooper and W.L. Barnes, The Basics of Plasmonics, Chapter 2 in Hanbook of Surface Science, Volume 4, Modern Plasmonics, Edited by A. A. Maradudin et.al., Elsevier, Amsterdam (2014)

[13] Junghyun Park, Kyoung-Youm Kim, Il-Min Lee, Hyunmin Na, Seung-Yeol Lee and Byoungho Lee, Trapping light in plasmonic waveguides, 18 January 2010 / Vol. 18, No. 2 / OPTICS EXPRESS 600, https://doi.org/10.1364/OE.18.000598

[14] Muamer Kadic, Sébastien Guenneau, Stefan Enoch, Paloma A. Huidobro, Luis Mart í n-Moreno, Francisco J. Garc í a-Vidal, Jan Renger and Romain Quidant, Transformation plasmonics, Nanophotonics 1 (2012): 51–64 © 2012 by Walter de Gruyter • Berlin • Boston. https://doi.org/1515/nanoph-2012-0011

[15] Kunal Shastri, Mohamed Ismail Abdelrahman and Francesco Monticone, Nonreciprocal and Topological Plasmonics, A Review, Photonics 2021, 8, 133, https://doi.org/10.3390/photonics8040133

[16] M. Born and E. Wolf. Principles of Optics. Cambridge University Press, Cambridge, sixth edition, 1980, p. 625

[17] J. Nkoma, R. Loudon, D.R. Tilley, Elementary properties of surface polaritons, Journal of Physics C: Solid State Physics, Vol. 7 (19), 3547-3559 (2001), https://doi.org 10.1088/0022-3719/7/19/015

[18] V.L. Ginzburg, “The propagation of electromagnetic waves in plasmas”, Pergamon Press, London, 1964, formula B 2.5, page 482.

[19] P. Kiełczyński, Direct Sturm–Liouville problem for surface Love waves propagating in layered viscoelastic waveguides, Applied Mathematical Modelling 53, 419–432 (2018) https://doi.org/10.1016/j.apm.2017.09.013

[20] S-Y. Yu, J-Q. Wang,X-C. Sun, F-K. Liu,C. He,H-H. Xu, M-H. Lu, J. Christensen, X-P. Liu,and Y-F. Chen, Slow Surface Acoustic Waves via Lattice Optimization of a Phononic Crystal on a Chip, Physical Review Applied, 14, 064008 (2020) https://doi.org/10.1103/PhysRevApplied.14.064008

[21] K. Deng, Z. He, Y. Ding, H. Zhao and Z. Liu, Surface-Plasmon-Polariton (SPP)-Like Acoustic Surface Waves on Elastic Metamaterials, arXiv:1408.2186v1 (2014)

[22] R. Zaccherini, A. Colombi, A. Palermo, V. K. Dertimanis , A. Marzani, H. R. Thomsen, B. Stojadinovic and E. N. Chatzi, Locally Resonant Metasurfaces for Shear Waves in Granular Media, Physical Review Applied, 13, 034055 (2020) https://doi.org/10.1103/PhysRevApplied.13.034055

[23] A.A. Maznev and V.E. Gusev, Waveguiding by a locally resonant metasurface, Physical Review B 92, 115422 (2015)

[24] Antonio Palermo & Alessandro Marzani, Control of Love waves by resonant metasurfaces, SCIENTIFIC REPORTS | (2018) 8:7234 | https://doi.org/101038/s41598-018-25503-8

[25] P. Kiełczyński, M. Szalewski, A. Balcerzak and K. Wieja, Group and Phase Velocity of Love Waves Propagating in Elastic Functionally Graded Materials, Archives of Acoustics, Vol. 40, No. 2, pp. 273–281 (2015) https://doi.org/10.1515/aoa-2015-0030

[26] P. Kiełczyński, New fascinating properties and potential applications of Love surface waves, Invited Speaker presentation at the International Ultrasonic Symposium of IEEE, September 11-16, 2021, Xi'an, China. Available on line: http://zbae.ippt.pan.pl/strony/publikacje.htm, (accessed 8 May 2023).

[27] Venu Gopal Achanta, Surface waves at metal-dielectric interfaces: Material science perspective, Reviews in Physics 5 (2020) 100041, https://doi.org/10.1016/j.revip.2020.100041

[28] Devi Taufiq Nurrohman and Nan-Fu Chiu, A Review of Graphene-Based Surface Plasmon Resonance and Surface-Enhanced Raman Scattering Biosensors: Current Status and Future Prospects, Nanomaterials 2021, 11, 216, https://doi.org/10.3390/nano11010216

[29] Yan Xu, Fei Wang, Yang Gao, Daming Zhang, Xiaoqiang Sun and Pierre Berini, Straight Long-Range Surface Plasmon Polariton Waveguide Sensor Operating at λ_0 = 850 nm, Sensors 2020, 20, 2507; https://doi.org/10.3390/s20092507